An Amalgam of Mg-Doped TiO2 Nanoparticles Prepared by Sol-Gel Method for Effective Antimicrobial and Photocatalytic Activity

N NITHYA (nithyanesakumar@gmail.com)
PSGR Krishnammal College for Women

S Gopi
SRMV College of Arts and Science

G Bhoopathi
PSG College of Arts and Science

Research Article

Keywords: Mg-TiO2 NPs, Structural properties, Reactive oxygen species, Antibacterial Activity, and Photocatalytic Activity

Posted Date: May 25th, 2021

DOI: https://doi.org/10.21203/rs.3.rs-550044/v1

Version of Record: A version of this preprint was published at Journal of Inorganic and Organometallic Polymers and Materials on September 15th, 2021. See the published version at https://doi.org/10.1007/s10904-021-02076-0.

An amalgam of Mg-Doped TiO_2 nanoparticles prepared by Sol-Gel method for effective Antimicrobial and Photocatalytic activity

N.Nithya[1], S. Gopi [2], G.Bhoopathi[3]

[1] Assistant Professor, Department of Physics, PSGR Krishnammal College for Women, Coimbatore- 641004.

[2] Assistant Professor, Department of Physics, SRMV College of Arts and Science, Coimbatore-641020.

[3] Associate Professor, Department of Physics, PSG College of Arts and Science, Coimbatore-641014.

Corresponding Author Email Id: nithyanesakumar@gmail.com

Abstract

In this study, undoped and Magnesium doped TiO_2 nanoparticles (Mg-TiO_2 NPs) were successfully synthesized via a simple sol-gel method cost-effectively. The prepared Mg- TiO_2 NPs were characterized by UV-Vis, FTIR, PL, XRD, FESEM, TEM, and EDAX. UV – Visible Spectroscopy showed that an increase in the optical bandgap concerning the concentration of dopant Mg increases. The bandgap values were found to be 3.57-3.54 eV. FTIR spectra showed that the presence of the characteristic stretching and bending vibrational band of Ti – O bonding at 468 cm-1 and shifts in vibrational bands were observed for Mg-TiO_2 NPs. PL spectra of Mg-TiO_2 NPs at different concentrations exhibit a strong UV emission band. X-ray diffraction confirmed the formation of the tetragonal anatase phase. The average crystallite size of prepared samples was found to be 22-19 nm. The average crystallite size of Mg- TiO_2 NPs decreases with increasing the concentration of dopant Mg. The FESEM and TEM analysis confirmed that the spherical morphology for both TiO_2 and Mg-TiO_2 NPs. SAED pattern confirms the crystalline nature of prepared samples. EDAX spectra confirm the presence of Ti, O, and Mg and confirm that Mg^{2+} ions are present in the TiO_2 lattices. The prepared samples were investigated against gram-positive (*B. subtilis* and *S. aureus*) and gram-negative (*P. eugenia* and *K. Pneumonia*) bacteria. The prepared samples showed potent antibacterial activity against gram-negative bacteria than the gram-positive bacteria. The prepared samples show the excellent photocatalytic degradation for Methylene blue.

Keywords: Mg-TiO_2 NPs, Structural properties, Reactive oxygen species, Antibacterial Activity, and Photocatalytic Activity.

1.1 Introduction

Nanotechnology has a wide range of applications such as electronics, catalysis, agriculture, optical communications, food packaging, etc. [1-3]. In the present era, nanomaterials have a greater interest in many fields because of change their optical and physical properties when particle size reduces to the nanoscale. The recent studies on semiconductor nanoparticles also suggested that optical bandgap becomes increased that as particle size decreased thereby change in its optical and electrical properties and thus making the nanomaterials suitable for several applications [4-6]. The performance of nanomaterials depending on the size and shape that are affected by the high surface to volume ratio. Different types of nanomaterials are used to enhance the optical, electrical, thermal, photocatalytic, antibacterial, and gas sensing properties [7, 8]. Fe_2O_3, WO_3, Bi_2O_3, MgO, ZnO, and TiO_2 are the most semiconductor nanomaterials that are used for photocatalyst, antibacterial applications, and safe for human beings, animals, and plants [9]. Among all the metal oxide nanomaterials, TiO_2 is an n-type semiconductor with a wide bandgap of 3.2 eV, UV light absorption, high chemical and thermal stability, and tetragonal structure [10]. TiO_2 has many applications in the field of biomedical, photocatalytic activity, antibacterial activity, gas sensors, solar cells, agriculture, water purification, textiles, food packaging, etc. [11].

TiO_2 occurs in three crystalline forms such as anatase, rutile, and brookite phase. These three forms have high refractive index values, which are 2.488, 2.609, and 2.583 respectively. Among these three forms, anatase is metastable, rutile is highly stable and brookite is unstable [12].

The anatase form is considered the most physically and chemically active phase of TiO_2 [13]. Shape and size-controlled synthesis of TiO_2 nanoparticles enhance its properties have been extensively studied in recent years [14]. There are several methods for the synthesis of TiO_2 nanoparticles such as sol-gel [15], wet chemical [16] co-precipitation [17] hydrothermal [18] ball milling [19] combustion [20], and biological method [21]. Among these methods, sol-gel is the most feasible method for the synthesis of TiO_2 nanoparticles because of its ability to control size and surface morphology. The sol-gel method has greater advantages, which include high purity, the low temperature required for synthesis, and excellent homogeneity of nanoparticles [22, 23].

TiO_2 nanoparticles also exhibit potent antibacterial properties that are useful in many biological applications.

Recently, there are increasing research in alkali metal ion (Al, Ca, Ce, Co, Cu, Fe, Ga, In, Mn, Mg, Nb, Sn, and Sr) doping method, which leads to change in physical and chemical properties of TiO_2 nanoparticles and enhances the antibacterial applications [24]. Among these metals, Mg-TiO_2 NPs exhibit potent antibacterial activity, because Mg^{2+} can be substituted into the Ti^{4+} ion owing to their smaller ionic radii. The smaller ionic radii of Mg^{2+} ion helpful to enhance the antibacterial efficiency [25]. The efficiency of antibacterial activity also depends on the structure of microbes.

Matsunaga et al [26] reported that TiO_2 nanoparticles showed good antimicrobial activity against Escherichia coli under UV irradiation. To overcome the drawbacks transition metals are doped to enhance the antibacterial efficiency under visible light. Karunakaran et al [27] demonstrated that Cu doped TiO_2 nanoparticles effective antibacterial activity towards *E. coli* and *S. aureus* under visible light. Meanwhile, they also studied Ni-TiO_2 NPs against gram-positive and gram-negative bacteria. Hamal et al [28] reported that Ag-doped TiO_2 nanoparticles enhance antibacterial activity against *E. coli* and *B. subtilis* and suggesting that the Ag is responsible for the enhancement of antibacterial efficiency. According to earlier reports, few works have been carried out on the effect of TiO_2 nanoparticles on antimicrobial activity [29].

However, to the best of our knowledge, only a few works have been reported on the antibacterial and Photocatalytic activity of Mg- TiO_2 NPs with different dopant concentrations. Moreover, Mg-TiO_2 NPs increase the concentration of oxygen species (ROS), and this oxygen species leading to the death of bacterial cells. The antibacterial activity of Mg-TiO_2 NPs depends on the variation in the doping concentration of Mg and the nature of bacterial species.

Herein, undoped and Mg-TiO_2 NPs were synthesized via the simple sol-gel method. The synthesized nanoparticles were investigated for structural, morphological, optical, antibacterial, and photocatalytic activity. The effect of various concentrations of Mg on the synthesis of Mg-TiO_2 NPs against gram-positive (*B. subtilis* and *S. aureus*) and gram-negative (*P. eugenia* and *K. Pneumonia*) bacteria under visible light. The photocatalytic degradation efficiency of Mg-TiO_2 NPs for Methylene Blue under UV irradiation was also studied.

2 Experimental Sections:

2.1 Preparation of undoped and Mg-TiO_2 NPs:

The high purity chemicals such as Titanium (IV) Isopropoxide ($Ti(OCH(CH_3)_2)_4$), Magnesium nitrate hexahydrate ($Mg(NO_3)_2$. $6H_2O$), and Sodium hydroxide (NaOH) were used as precursor without further purification.

For the preparation of Mg-TiO_2 NPs, 0.2g of Magnesium nitrate was prepared in 100 ml of deionized water. Subsequently, 5ml of Titanium (IV) Isopropoxide was prepared in 100 ml of Isopropyl Alcohol. Then the aqueous solution of Magnesium nitrate was added drop wise to form a homogenous mixture. After that, 0.8 M of aqueous NaOH solution was added dropwise to this homogenous mixture to form white precipitation. Then the homogenous mixture was stirred at room temperature for 5 hrs. Further, a homogenous mixture could age for 24 hrs. and then the white precipitate was washed with ethanol and distilled water to removed unwanted impurities present in the solution. Then the solution was centrifuged at 10000 rpm for 30 min. Finally, the precipitate was dried at 120^o C for 2 hrs and annealed at 450^o C for 5 hrs. to obtain Mg-TiO_2 NPs. The same procedure was followed for different concentrations of dopant Mg (0.4g, 0.6g and 0.8g). The obtained samples were ground with pestle and mortar and stored in an airtight container. The annealed samples were used for further studies. The same method was followed for TiO_2 nanoparticles without the addition of Magnesium nitrate.

2.2 Characterization:

The prepared undoped and Mg-TiO_2 NPs were examined using the following characterization techniques. UV-Visible absorption spectroscopy was obtained in the wavelength range 200 – 800 nm using a UV visible spectrophotometer (JASCO-V-770 Spectroscopy). Fourier transform infrared spectroscopy (FTIR) was carried out by using Bruker Alpha FTIR spectrometer at a wavenumber range of 400 cm-1 – 4000 cm-1. Photoluminescence spectroscopy of the prepared samples was analyzed using an FP-3800 spectrofluorometer. XRD diffraction pattern was analyzed using Bruker D8 Advance X-ray diffractometer with Cukα1 (l = 1.54060 Å) and Cukα2 (l = 1.54443 Å) radiation operating at 30mA and 45 kV at 2θ range of 10^o to 90^o. The Surface morphology of Mg-TiO_2 NPs was analyzed using a Field emission scanning

electron microscope (SIGMA HV-CARL ZEISS) and HRTEM images were taken in (JEOL – JEM -2010, JAPAN) with an accelerating voltage of 200kV.

2.3 Antibacterial experiment

Bacillus subtilis, Staphylococcus aureus, Pseudomonas aureginosa, and Klebsiella pneumonia were chosen as microbes for antibacterial assays. The antibacterial activity of undoped and Mg-TiO_2 NPs was tested using the disc diffusion method.

In brief, the microbes were cultivated in Müller-Hinton broth at 35°C ± 2°C on detour shuddering incubator (Remi, India) at 160 rpm. A pasture of microbial culture was arranged by dispersion of 10 mL culture broth of all test microbes on dense nutrient agar plates. The dishes were permitted to stand for 10-15 minutes for culture absorption. The 5 mm size discs/wells were perforated into the agar with the dome of sterilized micropipette tips. Using a spatula, 100 µg of undoped and Mg-TiO_2 NPs were kept into each of the discs on all plates. The microbes were inoculated to the culture media by inoculation in the petri dishes and incubated at 35±2°C for 24 hours for culturing bacteria. After incubation, the diameter of zone of inhibition were examined.

2.4 Photocatalytic degradation study

UV light irradiation of Photocatalytic degradation of undoped and Mg-TiO_2 NPs was analyzed for Methylene blue dye. In a typical photo degradation analysis, 50 ml of methylene blue solution was mixed with the appropriate amount of prepared samples (undoped and Mg-TiO_2 NPs) and stirred well in a glass beaker. The obtained suspension was kept under darkroom for 30 min and then irradiated with UV light with constant stirring. 3ml aqueous solution was extracted from the obtained suspension under UV irradiation with equal intervals of time. The absorption spectra of the solution were analyzed by UV visible spectrophotometer (JASCO-V-770 Spectroscopy). The photocatalytic rate constant for Methylene blue of prepared samples were calculated using the first-order equation

$$\ln (A_0/A) = kt \quad \rightarrow (1)$$

Where A_0 is the initial absorption, A is the absorption after a time t and k is the first-order rate constant.

3 Result and discussion

3.1 Influence of dopant Mg on crystal phase and crystallite size

XRD pattern of undoped and Mg-TiO_2 NPs exhibited peaks with tetragonal anatase phase reflections (JCPDS Card no. 78-2486) and possesses pure crystalline nature with trigonal planar O-3 and Ti-6 Octahedral coordination geometry [30]. Fig 1 illustrates the XRD pattern of undoped and Mg-TiO_2 NPs with different concentrations of Mg under the same condition. The patterns are recorded in 2θ in the range of 20º - 80º. The characteristics 2θ values are 25.30 º, 32.65 º, 37.59 º, 47.86 º, 53.81 º, 55.09 º, 62.57 º, 68.78 º, 70.30 º, 75.37º and corresponding hkl plane values are (1 0 1), (0 0 2), (0 0 4), (2 0 0), (1 0 5), (2 1 1), (2 0 4), (1 1 5), (2 2 0) and (2 1 5) respectively. The prominent peak at 25º indicates the crystalline nature of prepared samples. The tetragonal anatase crystalline nature of TiO_2 remains unaffected with the amalgamation of Mg into TiO_2 lattice. When increasing the doping concentration Mg, the difference in the intensity of the diffraction peaks and minor shifts in the peak occurs this indicates the reduction of crystalline size and increase of volume of unit cell. The ionic radii of Mg^{2+} (0.71 Å) ion and Ti4+ (0.62 Å) are very near with each other, hence Mg^{2+} can easily enter the TiO_2 lattice [31]. The similar ionic radii of dopant arise the possibility of Mg^{2+} enter the TiO_2 lattice through substitution mode. Thereby, doping through the substitution model involves the direct substitution of metal ions to occupy their position in the lattice. The peak broadening and no impurity peak occur when increasing the dopant concentration Mg, which indicates a reduction of crystallite size, and all the dopant elements cannot enter into the TiO_2 lattice and some of them are formed on the surface of TiO_2 NPs.

The Scherrer's formula was used to calculate the crystallite size of undoped and Mg-TiO_2 NPs as follows [32],

$$D = k\lambda / \beta \cos \theta \quad \rightarrow (2)$$

Where K is the Scherrer's constant, β is the full wave half maximum (FWHM) of the X-ray diffraction (radians), λ is the wavelength of the X-ray (nm) and θ is the diffraction angle. The assessed crystallite size of as-prepared nanoparticles was found to be 22 nm, 21 nm, 20.4 nm, 20 nm, and 19.6 nm respectively. The crystallite size is found to decrease with Mg-TiO_2 NPs

increases which are due to Mg^{2+} ion is incorporated into the TiO_2 lattice. The doping with Mg with TiO_2 also increases the oxygen species and these oxygen species are responsible to enhance the antibacterial and photocatalytic activity.

The lattice constant of the tetragonal anatase phase of undoped and Mg-TiO_2 NPs was calculated using the formula,

$$\frac{1}{d^2} = \frac{h^2 + k^2}{a^2} + \frac{l^2}{c^2} \quad \rightarrow (3)$$

Where d is the interplanar spacing, a and c are lattice constants, h k and l are the miller indices. Positional parameter (u), bond length (l), and volume of the unit cell (V) of as-prepared samples were obtained using the following relation.

$$\mathbf{V = a^2 c} \quad \text{Å}^3 \quad \rightarrow (4)$$

$$\mathbf{L} = \sqrt{\frac{\mathbf{a^2}}{\mathbf{3}} + (\frac{\mathbf{1}}{\mathbf{2}} - \mathbf{u})^2 \mathbf{c^2}} \quad \rightarrow (5)$$

$$\mathbf{u} = \frac{\mathbf{a^2}}{\mathbf{3c^2}} + \mathbf{0.25} \quad \rightarrow (6)$$

The obtained value of crystallite size, lattice parameter, positional parameter, bond length, and unit cell volume of undoped and Mg-TiO_2 NPs are summarized in table 1. As presented in table 1, the crystallite size of as-prepared nanoparticles decreases when increases the dopant concentration Mg and also a slight variation in the positional parameter, bond length, and volume of the unit cell values, this might be due to the incorporation of Mg^{2+} ion into the TiO_2 lattice.

3.2 Morphology and elemental Analysis of as-prepared nanoparticles

The surface morphology of the as-prepared undoped and Mg-TiO_2 NPs was examined using FESEM analysis and results are shown in fig 2. The morphology of as-prepared nanoparticles shows a spherical shape. The particle size of undoped and Mg-TiO_2 NPs is around 25 nm. From the XRD results, it can be inferred that the crystallite size is less than the particle size and it proves that the prepared nanoparticle is in crystalline nature. In addition, the aggregation and agglomeration occur in the prepared nanoparticles and it is shown in the FESEM images. The decrease in agglomeration can be attributed to the increasing the dopant concentration Mg and particle size also decreases. The crystalline is defined as the lowest even crystallographic unit based on the disorientation of the adjacent atoms and the nanoparticle consists of more than one crystalline with dissimilar direction. Here, particle size obtained from FESEM results is in good agreement with XRD results and this also actually happens in the case of nanoparticles. The high crystalline nature of prepared nanoparticles enhances the antibacterial and photocatalytic activity.

The quantitative microanalysis of undoped and Mg-TiO_2 NPs was analyzed by EDAX and shown in fig 3 and the results are listed in table 2. The results from the EDAX spectra confirm the presence of Mg, Ti, and O and the percentage of Mg increases with increasing the dopant concentration, thereby decreasing the concentration of Ti into the TiO_2 lattice. Furthermore, the percentage of Mg and Ti indicates the substitution mode of doping on the surface of the TiO_2 lattice. The results also show that the increase in the percentage of oxygen on the surface of TiO_2 attributed to enhances the antibacterial and photocatalytic activity. No other additional impurities are detected in the EDAX spectra.

Fig 4(A-B) depicts the TEM analysis of undoped and Mg-TiO_2 NPs. The results illustrate the prepared nanoparticles are spherical. The entire prepared sample shows a uniform spherical morphology with well crystalline nature. Fig (C-D) indicates the lattice fringes of undoped and Mg-TiO_2 NPs. d -spacing values are calculated using the relation [33].

$$Ll = dR \qquad \rightarrow (7)$$

Where L is the camera length (120 nm), l is the wavelength of the electron beam and R is the radius diffraction ring respectively. d - spacing values of undoped and Mg-TiO_2 NPs were found to be 0.239 nm and 0.268 nm respectively which corresponds to the (1 0 1) tetragonal anatase phase of TiO_2 nanoparticles. Lattice spacing values were found to be slight increases when Mg-TiO_2 NPs which are ascribed to the imperfections in TiO_2 lattice due to metal ion doping [34]. The intensity of the crystalline phase of TiO_2 nanoparticles was decreased which are well-matched with intensity peaks of XRD results. The crystallinity of as-prepared samples was assessed using the selected area diffraction pattern (SAED) and portrayed in fig 4 (E-F). The ring pattern confirms the anatase crystalline nature of as-prepared nanoparticles and a bright spot indicates the formation of high crystallinity nature of undoped and Mg-TiO_2 NPs (1 0 1) anatase phase. The mean particle size of undoped and Mg-TiO_2 NPs was obtained to be 24.6 nm and 21.9 nm respectively. The assessed particle size is in good accord with the crystalline size of XRD results. From the TEM results, particle size decreases the increasing the dopant concentration which is due to Mg^{2+} ion is incorporated into the TiO_2 lattice. The smaller particle size improves photocatalytic activity.

3.3 Optical properties and bandgap assessment of as-prepared nanoparticles.

The optical properties of as-prepared nanoparticles were examined using UV-visible absorption spectroscopy carried out at room temperature and depicted in fig 5. Generally, TiO_2 nanoparticles tend to absorb UV light of bandgap 3.2 eV. The absorption peak exhibit UV cutoff wavelength which is attributed to photoexcitation of electron from the valence band (formed from 2p orbital of the oxide anion) to conduction band (formed from the 3d orbitals of the Ti^{4+} cation [35]. The shift in the absorption edge was observed for Mg-TiO_2 NPs which are ascribed to the acceptor tendency of Mg in the TiO_2 and creation of additional state within the TiO_2 lattice which leads to reducing the bandgap.

To estimate the bandgap of as-prepared samples, Tauc's formula is used from UV visible spectra [36].

$$(\alpha h\nu) = A(h\nu - E_g)^n \quad \rightarrow (8)$$

Where **α**- is the linear absorption coefficient, hν is the energy of a photon; A is the proportionality constant and E_g is the bandgap energy respectively. Here n is the characteristics of transition in a semiconductor nanoparticle. And n =1/2 for direct bandgap and n = 2 for indirect bandgap. The bandgap values of undoped and Mg-TiO_2 NPs were achieved by scheming a linear region in the plots $(\alpha h\nu)^{1/2}$ to the crossing with energy axis (E/eV) and shown in fig 6. The estimated bandgap energy of TiO_2 nanoparticles is 3.57 eV and bandgap energy values decrease from 3.57 eV to 3.54 eV respectively. The decrease in bandgap due to an increase in photo absorption and this might be enhancing the photocatalytic activity.

The structural defects and crystal properties of as-prepared samples were analyzed using PL analysis with an excitation wavelength of 345nm at room temperature. Photoluminescence (PL) spectra of undoped and Mg-TiO_2 NPs depicted in fig 7. PL spectra exhibit a peak at 388 nm, 458 nm, and 535nm respectively. There is no new peak arises for Mg-TiO_2 NPs. The prominent peak at 388 nm is due to UV emission and self-blocking excitons near the band edge of TiO_2. The UV emission band arises due to the recombination of electron-hole pair which is near band edge emission (NBE). The intensity of the peak slightly increases when Mg added to TiO_2 which is due to an increase in electron-hole pair recombination. The shifts in peak also due to a decrease in particle size and bandgap energy of as-prepared nanoparticles. The highest peak at 388 nm also confirms the formation crystalline nature of TiO_2. Another peak at 458 nm due to deep level emission from the structural defects such as oxygen vacancies and impurities on the surface of TiO_2 [37]. PL spectra were observed between 300 to 550 nm this might be due to intrinsic and extrinsic structural defects. This may because when an electron from the valence band to the conduction band and forms the electron-hole pair. The low-intensity peak at 535 nm corresponds to green emission and it can be arising due to charge carriers formed after the recombination process take place and oxygen species on the surface of TiO_2 nanoparticles. The increase in oxygen vacancies happens with increasing dopant Mg and this may cause development in photocatalytic activity.

The different modes of vibration of as-prepared nanoparticles can be studied by using Fourier Transforms Infrared Technique (FTIR) and depicted in fig 8. The broadband at 3748 cm^{-1} could be attributed to the hydroxyl group of stretching mode of vibration of TiO_2 nanoparticles and forms oxygen vacancies in the occurrence of water. The presence of the OH group also increases

the photocatalytic activity since the OH group helps as a scavenger for photogenerated charge carriers [38]. The absorption band at 2936 cm^{-1} and 2348 cm^{-1} related to symmetric and asymmetric vibration of -CH_2 and -CH_3 groups. The band at 1626 cm^{-1} related to characteristics of amide I and II and indicating the formation of the band at an infrared region which increases the surface hydroxylation of TiO_2 nanoparticles when doping with Mg. FTIR band includes 1544 cm^{-1} corresponds to C-N stretching modes of vibration. The peak at 1358 cm^{-1} resembles to C-H stretching vibration [39, 40, 41]. The absorption peak appears at 468 cm^{-1} corresponds to Ti-O stretching modes of vibration or antisymmetric Ti-O-Ti modes of vibration of TiO_2 nanoparticles. This peak plays a significant role in enhancing photocatalytic activity.

4. Antibacterial activity

Generally, the antibacterial activity of nanoparticles depends on various factors such as phase formation, particle size, surface morphology, specific surface area, chemical composition, and surface hydroxyl groups [42, 43]. The antibacterial activities of Pure and different concentrations of Mg-TiO_2 NPs were investigated against *Bacillus subtilis, Staphylococcus aureus, Pseudomonas aureginosa,* and *Klebsiella pneumonia* by disc diffusion method. The zone of inhibition was increased when increasing the doping concentration Mg as shown in Fig 9. Mg-TiO_2 NPs (0.8g) exhibited the best antibacterial activities of both gram-negative and gram-positive bacteria as shown in Fig 10. Moreover, gram-negative bacteria are comparatively more sensitive to Mg-TiO_2 NPs than gram-positive bacteria. This might be due to the difference in the cell structure of bacteria. As the gram-positive bacteria have a thick lipopolysaccharide cell membrane as related to gram-negative bacteria. And lipopolysaccharide cell membrane acts as an additional barrier for undoped and Mg-TiO_2 NPs, leading to relatively lower antibacterial activities for gram-positive bacteria.

The several killing mechanisms of TiO_2 nanoparticles explained in literature such as ROS generation, superficial tension leads to cell damage, Ti^{2+} ion penetrates cell membrane leads to damage of cell wall, hole creation, and leakage of intracellular electrolytes [44,45]. Amongst, ROS creation was mostly used to describe the antibacterial activities of TiO_2 nanoparticles. According to the ROS creation of TiO_2 nanoparticles, additional electron-hole pairs might be formed on the surface of nanoparticles. ROS creation mainly consists of hydroxyl radicals,

hydrogen peroxide (H_2O_2), and superoxide anion radicals [46]. Furthermore, TiO_2 nanoparticles bind with the external microbial membrane and enter the cell wall. This damage the cell wall, DNA, lipids, and protein synthesis and leads to bacteria viability [47]. The killing mechanism of TiO_2 nanoparticles is given below [48].

$$TiO_2 \longrightarrow TiO_2 * + e^- + h^+ \quad \rightarrow (9)$$

$$H_2O + h+ \longrightarrow OH* + H^+ \quad \rightarrow (10)$$

$$O_2\,(ads) + e^- \longrightarrow O_2\text{-}^* \quad \rightarrow (11)$$

Carol López de Dicastillo *et al*. [49] reported the higher antibacterial activity of TiO_2 nanosphere against *Escherichia coli* and *Staphylococcus aureus*. Zimbone et al. [50] reported the antibacterial activity of TiO_2 nanoparticles against gram-negative bacteria *Escherichia coli*. The antibacterial activities of undoped and Mg-TiO_2 NPs also depend on the crystallite and morphology. The efficacy of antibacterial activities of undoped and Mg-TiO_2 NPs are shown in table 1. The results reveal that antibacterial activities of Mg-TiO_2 NPs are higher for gram-negative bacteria than gram-positive bacteria. When increasing the concentration of Mg, the antibacterial activities also increase.

In this study, Mg-TiO_2 NPs (0.8g) exhibited higher antibacterial activity because of the smaller crystallite size with a larger surface area. In addition, Mg also increases the oxygen vacancies in ROS generation to enhance the antibacterial activity. The doping of Mg with TiO_2 nanoparticles leads to the variation in particle size, morphology, and solubility of Ti^{2+}. The results reveal that Mg-TiO_2 NPs will be a promising candidate for a potential drug delivery system to cure some significant infections in the future.

5. Photocatalytic activities

UV irradiated Photocatalytic degradation of Methylene Blue for undoped and Mg-TiO_2 NPs are depicted in fig 11. Mg-TiO_2 NPs show enhanced Photocatalytic degradation efficiency than TiO_2 nanoparticles. The photocatalytic reactions are initiated from $OH\cdot$ and O^{2-} radicals formed on the surface of TiO_2 nanoparticles [51]. The photocatalytic mechanism of as prepared samples were shown in fig 12.

$$TiO_2\ Mg + h\upsilon \longrightarrow e - (\mathbf{CB}) + h^+ (\mathbf{VB}) \rightarrow (12)$$

The Photocatalytic degradation efficiency of TiO_2 nanoparticles from 0 – 45 min was found to be 68%, 74%, and 86% and 76%, 88%, and 95% respectively for Mg-TiO_2 NPs. From the result of photodegradation efficiency, Mg-TiO_2 NPs exhibit potent performance than Pure TiO_2 nanoparticles. The higher photocatalytic efficiency for Mg-TiO_2 NPs due to smaller crystallite size and higher bandgap energy than TiO_2 nanoparticles. Because the crystallite size and bandgap energy play an important role in photocatalytic activity. And also dopant Mg modified the physical and chemical properties of TiO_2 nanoparticles. The reduced crystallite size of Mg-TiO_2 NPs nanoparticles also decreases the recombination of photogenerated electron-hole pair and it also enhances the photocatalytic activity. The higher concentration of Mg-TiO_2 NPs shows enhanced photocatalytic activity than TiO_2 nanoparticles and this is because of the charge separation efficiency of electron-hole pair. And also, when Mg-TiO_2 NPs could form surface defects and oxygen species on the surface of prepared nanoparticles. The enhanced photocatalytic activity of Mg-TiO_2 NPs is due to smaller crystallite size and bandgap energy which was confirmed by XRD and UV analysis respectively. The calculated rate constant of TiO_2 nanoparticles were 0.023, 0.035, and 0.054 min^{-1} after 45 min and 0.026, 0.038, and 0.059 min^{-1} for Mg-doped TiO_2 were and shown in fig 13. The higher rate constant was obtained for Mg-doped TiO_2 nanoparticles and this is due to higher bandgap energy which causes higher redox potential for photogenerated electron-hole pair which extensively enhances the photocatalytic activity.

The photodegradation efficiency of undoped and Mg-TiO_2 NPs over 5 cycles for Methylene Blue over 45 min is shown in fig 14. The efficiency of TiO_2 nanoparticles was decreased from 86% to 76% and 95% to 92% for Mg-TiO_2 NPs. The lower efficiency of TiO_2 nanoparticles is due to the photo corrosion phenomenon during photocatalytic reactions. On the other hand, doping with alkali metals increases the photocorrosive resistance and increases the chemical stability of TiO_2 nanoparticles during photocatalytic reactions. The photo corrosion phenomenon in the TiO_2 nanoparticles can be occur using the relations [52].

$$TiO_2 + 2h+ \longrightarrow Ti^{2+} + O_2 \rightarrow (13)$$

The photo corrosion is caused by the reaction of oxygen species and holes present on the surface of TiO_2 nanoparticles. According to XRD results, Mg-TiO_2 NPs leads to increases in the oxygen species and also increases the chemical stability of photocatalytic reactions.

Conclusion

Bestowing to this work, Pure and Mg doped TiO_2 nanoparticles were synthesized by facile sol- gel technique. The synthesized nanoparticles were characterized by XRD, FESEM with EDAX, TEM, UV, FTIR and PL analysis. The XRD spectrum confirms the presence of tetragonal anatase phase of TiO_2 nanoparticles with lesser crystallite size. When crystallite size decreases with increase the dopant concentration of Mg. FESEM and TEM analysis also confirms the various sized smooth spherical morphology of TiO_2 nanoparticles was achieved from this method. EDAX analysis also confirms the presence of Ti, O and Mg without any other impurities. Red shift in UV analysis confirms the incorporation of Mg into TiO_2 nanoparticles. PL analysis confirms the UV emission and green emission region and change in intensity of the peak confirms the incorporation of Mg. The presence of functional group was confirmed by FTIR spectrum. The prepared nanoparticles were also investigated for antimicrobial and photocatalytic activity. Pure and Mg doped TiO_2 nanoparticles show potent killing effect against the gram-negative bacteria than the gram-positive bacteria. The difference in killing effect due to cell structure and smaller crystallite size. Mg doped TiO_2 nanoparticles shows higher degradation efficiency than TiO_2 nanoparticles and this is because of smaller crystallite size. This method was a simple, coat effective, good dopant to preparation of low crystallite size TiO_2 nanoparticles.

References

1. Kavitha K.S., Baker S., Rakshith D., Kavitha H.U., Yashwantha Rao H.C., Harini B.P., Plants as Green Source Towards Synthesis of Nanoparticles, *Int. Research J. Bio. Sci.,* **2**, (2013), 66-77.
2. Abhilash M., Potential Applications of Nanoparticles, *Int. J. Pharm. Biol. Sci.*, **1**, (2010), 1-12.
3. Nagarajan S., Arumugam K. K., Extracellular Synthesis of Zinc Oxide Nanoparticle Using Seaweeds of Gulf of Mannar, India, *J. Nanobiotechnol*, **11**, (2013), 1-39.
4. Hameed, A. S., Karthikeyan, C., Sasikumar, S., Senthilkumar, V.,Kumaresan, S., & Ravi, G. , Journal of Materials Chemistry B, 1, (2013). 5950–5962.
5. Hameed, A. S., Karthikeyan, C., Senthilkumar, V., Kumaresan, S., & Sasikumar, S. , Materials Science and Engineering: C, 52, (2015), 171–177.
6. Hameed, A. S., Karthikeyan, C., Ahamed, A. P., Thajuddin, N., Alharbi, N. S., & Alharbi, S. A. , Ravi G Scientific reports., 6, (2016), 24312.
7. A. Sirelkhatim, S. Mahmud, A. Seeni, N.H.M. Kaus, L.C. Ann, S.K.M. Bakhori, H. Hasan, D. Mohamad, Review on zinc oxide nanoparticles: antibacterial activity and toxicity mechanism, Nano-Micro Lett. 7 (2015) 219–242
8. J.H. Li, R.Y. Hong, M.Y. Li, H.Z. Li, Y. Zheng, J. Ding, Effects of ZnO nanoparticles on the mechanical and antibacterial properties of polyurethane coatings, Prog. Org. Coat. 64, (2009) 504–509.
9. Alhadrami HA, Al-Hazmi F. Antibacterial Activities of Titanium Oxide Nanoparticles. J Bioelectron Nanotechnol , 2, 2017, 5.
10. Banu S., Vishnu V., Jamuna K., Kurian G.A., Physiochemical Investigation and Biovaluation of TiO2 Nanocrystals Synthesized by Chemical and Green Route*, Int. J. Pharm. Pharm. Sci.,* **6,** (2014), 396-400.
11. Periyat P., McCormack D.E., Hinder S.J., Pillai S.C., One-Pot Synthesis of Anionic (Nitrogen) and Cationic (Sulfur) Codoped High-Temperature Stable, Visible Light Active, Anatase Photocatalysts, *J. Phys. Chem. C*, **113**, (2009), 3246-3253.

12. Muhammad, Bilal Bibi, Ambreen Javed, Ali Irfana, Shahid, Effects of Solvent on the Structure and Properties of Titanium Dioxide Nanoparticles and Their Antibacterial Activity, Iran. J. Chem. Chem. Eng., Vol. 38, No. 4, (2019) 261-272.
13. Chen L., Rahme K., Holmes J.D., Morris M.A., Slater N.K., Non-Solvolytic Synthesis of Aqueous Soluble TiO2 Nanoparticles and Real-Time Dynamic Measurements on the Nanoparticle Formation, *Nanoscale res. lett.*, **7,** (2012)): 1-10.
14. Oon Lee Kang, Azizan Ahmad,Usman Ali Rana, and Nur Hasyareeda Hassan, Sol-Gel Titanium Dioxide Nanoparticles: Preparation and Structural Characterization, Journal of Nanotechnology Volume 2016, Article ID 5375939, 7 pages.
15. Feinle, A., Elsaesser, M. S., and Hüsing, N., Sol–gel synthesis of monolithic materials with hierarchical porosity. Chemical Society Reviews, 45, (2016), 3377–3399.
16. Rucha Desai, Sanjeev K. Gupta, Shree Mishra, P. K. Jha,§ And A. Pratap, The Synthesis Of Tio2 Nanoparticles By Wet-Chemical Method And Their Photoluminescence, Thermal And Vibrational Characterizations: Effect Of Growth Condition, International Journal of Nanoscience Vol. 10, No. 6, (2011), 1249-1256.
17. Weeraman Buraso, Vichuda Lachom, Porntip Siriya and Paveena Laokul, Synthesis of TiO2 nanoparticles via a simple precipitation method and photocatalytic performance, Mater. Res. Express 5, (2018), 115003.
18. Hadja Fatima Mehnane, Changlei Wang, Kiran Kumar Kondamareddy, Wenjing Yu, Weiwei Sun, Haimin Liu, Sihang Bai, Wei Liu, Shishang Guo and Xing-Zhong Zhao, Hydrothermal synthesis of TiO2 nanoparticles doped with trace amounts of strontium, and their application as working electrodes for dye sensitized solar cells: tunable electrical properties & enhanced photo-conversion performance, RSC Adv., 7, (2017), 2358.
19. J. O. Carneiro , S. Azevedo , F. Fernandes , E. Freitas , M. Pereira , C. J. Tavares , S. Lanceros-Me´ndez , V. Teixeira, Synthesis of iron-doped TiO2 nanoparticles by ball-milling process: the influence of process parameters on the structural, optical, magnetic, and photocatalytic properties, J Mater Sci , 49, (2014), 7476–7488.
20. Mostafa Y. Nassar, Eman I. Alia and Essam S. Zakaria, Tunable auto-combustion preparation of TiO2 nanostructures as efficient adsorbents for the removal of an anionic textile dye, RSC Adv., 7, (2017), 8034.

21. Chidambaram Jayaseelan , Abdul Abdul Rahuman , Selvaraj Mohana Roopan , Arivarasan Vishnu Kirthi , Jayachandran Venkatesan , Se-Kwon Kim , Moorthy Iyappan , Chinnadurai Siva, Biological approach to synthesize TiO2 nanoparticles using Aeromonas hydrophila and its antibacterial activity, Spectrochimica Acta Part A: Molecular and Biomolecular Spectroscopy 107, (2013), 82–89.
22. Kondratiev V.I., Kink I., Romanov A.E., Low Temperature Sol-Gel Technique for Processing Al- Doped Zinc Oxide Films, *Mater. Phys. Mech.*, **17**, (2013), 38-46.
23. Ullattil, S. G., & Periyat, P, Sol-Gel Synthesis of Titanium Dioxide. Sol-Gel Materials for Energy, Environment and Electronic Applications, (2017), 271–283.
24. Qianfei Zhao, Mei Wang, He Yang, Dai Shi, Yuzheng Wang, Preparation, characterization and the antimicrobial properties of metal ion-doped TiO2 nano-powders, ceramic international, 44, (2018), 5145-5154.
25. Shakir, S., Abd-ur -Rehman, H. M., Yunus, K., Iwamoto, M., & Periasamy, V., Fabrication of un-doped and magnesium doped TiO2 films by aerosol assisted chemical vapor deposition for dye sensitized solar cells. Journal of Alloys and Compounds, 737, (2018), 740–747.
26. T. Matsunaga, R. Tomoda, T. Nakajima and H. Wake, "Photoelectrochemical Sterilization of Microbial Cells by Semiconductor Powders," FEMS Microbiology Letters, 29, (1985), 211-214.
27. C.Karunakaran, G. Abiramasundari, P. Gomathisankar, G. Manikandan, V. Anandi, J. Colloids Interface. Sci., 352, (2010), 68–74.
28. D. B. Hamal, J. A. Haggstrom, G. L. Marchin, M. A. Ikenberry, K. Hohn, K. J. Klabunde, *Langmuir* **,** *26*, (2010), 2805
29. Arora, B., Murar, M., & Dhumale, V., Antimicrobial potential of TiO2 nanoparticles against MDR Pseudomonas aeruginosa. Journal of Experimental Nanoscience, 10, (2014), 819–827.
30. Dubey, R. S., & Singh, S., Investigation of structural and optical properties of pure and chromium doped TiO 2 nanoparticles prepared by solvothermal method. Results in Physics, 7, (2017), 1283–1288.
31. Olowoyo, J. O., Kumar, M., Singhal, N., Jain, S. L., Babalola, J. O., Vorontsov, A. V., & Kumar, U. , Engineering and modeling the effect of Mg doping in TiO2 for enhanced

photocatalytic reduction of CO2 to fuels. Catalysis Science & Technology, 8, (2018), 3686–3694.

32. Arasi, S. E., Madhavan, J., & Antony Raj, M. V., Effect of samarium (Sm3+) doping on structural, optical properties and photocatalytic activity of titanium dioxide nanoparticles. Journal of Taibah University for Science, 12, (2018), 186–190.
33. Gopinath Kasi, Jongchul Seo, Influence of Mg doping on the structural, morphological, optical, thermal, and visible-light responsive antibacterial properties of ZnO nanoparticles synthesized via co-precipitation, Material science and Engineering B, 98, (2019), 717-725.
34. Mani Rahulan K, Ganesan S, Aruna P, Synthesis and optical limiting studies of Au-doped TiO2 nanoparticles. Adv Nat Sci: Nanosci Nanotechnol, 2, (2011), 025012.
35. Li Xuemin, Guo Zhengkai, He Tao, The doping mechanism of Cr into TiO2 and its influence on the photocatalytic performance. Phys Chem Chem Phys, 15, (2013), 20037–45.
36. F. N. Jiménez-García, B. Segura-Giraldo, E. Restrepo-Parra, G.A. López-López, Synthesis of TiO2 thin films by the SILAR method and study of the influence of annealing on its structural, morphological and optical properties, Ingeniare. Revista chilena de ingeniería, 23, (2015), 622-629.
37. Sharma, R., Sarkar, A., Jha, R., Sharma, A. K., & Sharma, D, Sol-Gel Mediated Synthesis of TiO2 Nanocrystals: Structural, Optical and Electrochemical Properties. International Journal of Applied Ceramic Technology, Int J Appl Ceram Technol. 17, (2020), 1400–1409.
38. Ali, T., Tripathi, P., Azam, A., Raza, W., Ahmed, A. S., Ahmed, A., & Muneer, M, Photocatalytic performance of Fe-doped TiO2nanoparticles under visible-light irradiation. Materials Research Express, 4, (2017), 015022.
39. Anuja Bokare , Mrinal Pai , Anjali A. Athawale, Surface modified Nd doped TiO2 nanoparticles as photocatalysts in UV and solar light irradiation, Solar Energy 91 (2013) 111–119.
40. Manish Hudlikar, Shreeram Joglekar, Mayur Dhaygude , Kisan Kodam, Green synthesis of TiO2 nanoparticles by using aqueous extract of Jatropha curcas L. latex, Materials Letters 75 (2012) 196–199.

41. Andrea León, Patricia Reuquen , Carolina Garín , Rodrigo Segura , Patricio Vargas , Paula Zapata and Pedro A. Orihuela, FTIR and Raman Characterization of TiO2 Nanoparticles Coated with Polyethylene Glycol as Carrier for 2-Methoxyestradiol, Appl. Sci.7, (2017), 49.
42. Wu, B., Huang, R., Sahu, M., Feng, X., Biswas, P., & Tang, Y. J., Bacterial responses to Cu-doped TiO2 nanoparticles, Science of The Total Environment, 408, (2010), 1755–1758.
43. T. Ali, Ateeq Ahmed, Umair Alam, Imran Uddin, P. Tripathi, M. Muneer, Enhanced photocatalytic and antibacterial activities of Ag-doped TiO2 nanoparticles under visible light, Materials Chemistry and Physics, 212, (2018), 325-335.
44. Jiang, X., Yang, L., Liu, P., Li, X., & Shen, J., The photocatalytic and antibacterial activities of neodymium and iodine doped TiO2 nanoparticles. Colloids and Surfaces B: Biointerfaces, 79, (2010), 69–74.
45. Ananpattarachai, J., Boonto, Y., & Kajitvichyanukul, P., Visible light photocatalytic antibacterial activity of Ni-doped and N-doped TiO2 on Staphylococcus aureus and Escherichia coli bacteria. Environmental Science and Pollution Research, 23, (2015), 4111–4119.
46. Zhao, Q., Wang, M., Yang, H., Shi, D., & Wang, Y., Preparation, characterization and the antimicrobial properties of metal ion-doped TiO2 nano-powders. Ceramics International, 44, (2018), 5145–5154.
47. Gouri Venkatesh Anehosur, Raghvendra D. Kulkarni, Medha Ganesh Naik and Ramesh K. Nadiger, Synthesis and Determination of Antimicrobial Activity of Visible Light Activated TiO2 Nanoparticles with Polymethyl Methacrylate Denture Base Resin Against Staphylococcus Aureus, Anehosur J Gerontol Geriatric Res, 1, (2012), 1000103.
48. Mohsen Behpour, Maryam Chakeri, Ag-doped TiO2 Nanocomposite Prepared by Sol Gel Method: Photocatalytic Bactericidal Under Visible Light and Characterization, JNS, 2, (2012) 227-234.
49. Carol López de Dicastillo, Cristian Patiño, María José Galotto , Yesseny Vásquez-Martínez, Claudia Torrent, Daniela Alburquenque , Alejandro Pereira, and Juan Escrig, Novel hollow titanium dioxide nanospheres with antimicrobial activity against resistant bacteria, Beilstein J. Nanotechnol. 10, (2019) 1716–1725.

50. Zimbone, M., Buccheri, M. A., Cacciato, G., Sanz, R., Rappazzo, G., Boninelli, S., Grimaldi, M. G., Photocatalytical and antibacterial activity of TiO2 nanoparticles obtained by laser ablation in water. Applied Catalysis B: Environmental, 165, (2015), 487–494.

51. Rani P. Barkul, Meghshyam K. Patil, Satish M. Patil, Vrushali B. Shevale, Sagar D. Delekar, Sunlight-assisted photocatalytic degradation of textile effluent and Rhodamine B by using iodine doped TiO2 nanoparticles, Journal of Photochemistry and Photobiology A: Chemistry 349, (2017), 138–147.

52. Joshua O. Olowoyo, Manoj Kumar , Nikita Singhal , Suman L. Jain , Jonathan O. Babalola , Alexander V. Vorontsov, Umesh Kumar, Engineering and Modeling the Effect of Mg Doping in TiO2 for Enhanced Photocatalytic Reduction of CO2 to Fuels, *J. Name*., 2013, 00, 1-3.

Figures

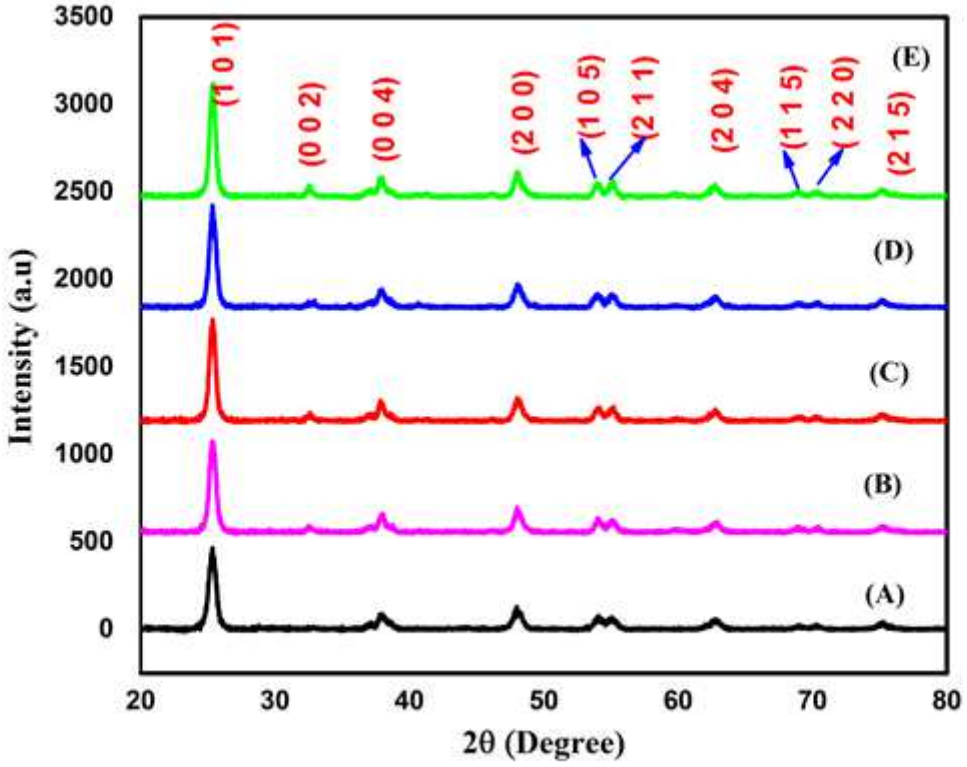

Figure 1

XRD spectra of A) undoped and Mg-TiO2 NPs B)0.2g C)0.4g D) 0.6g E)0.8g of Mg

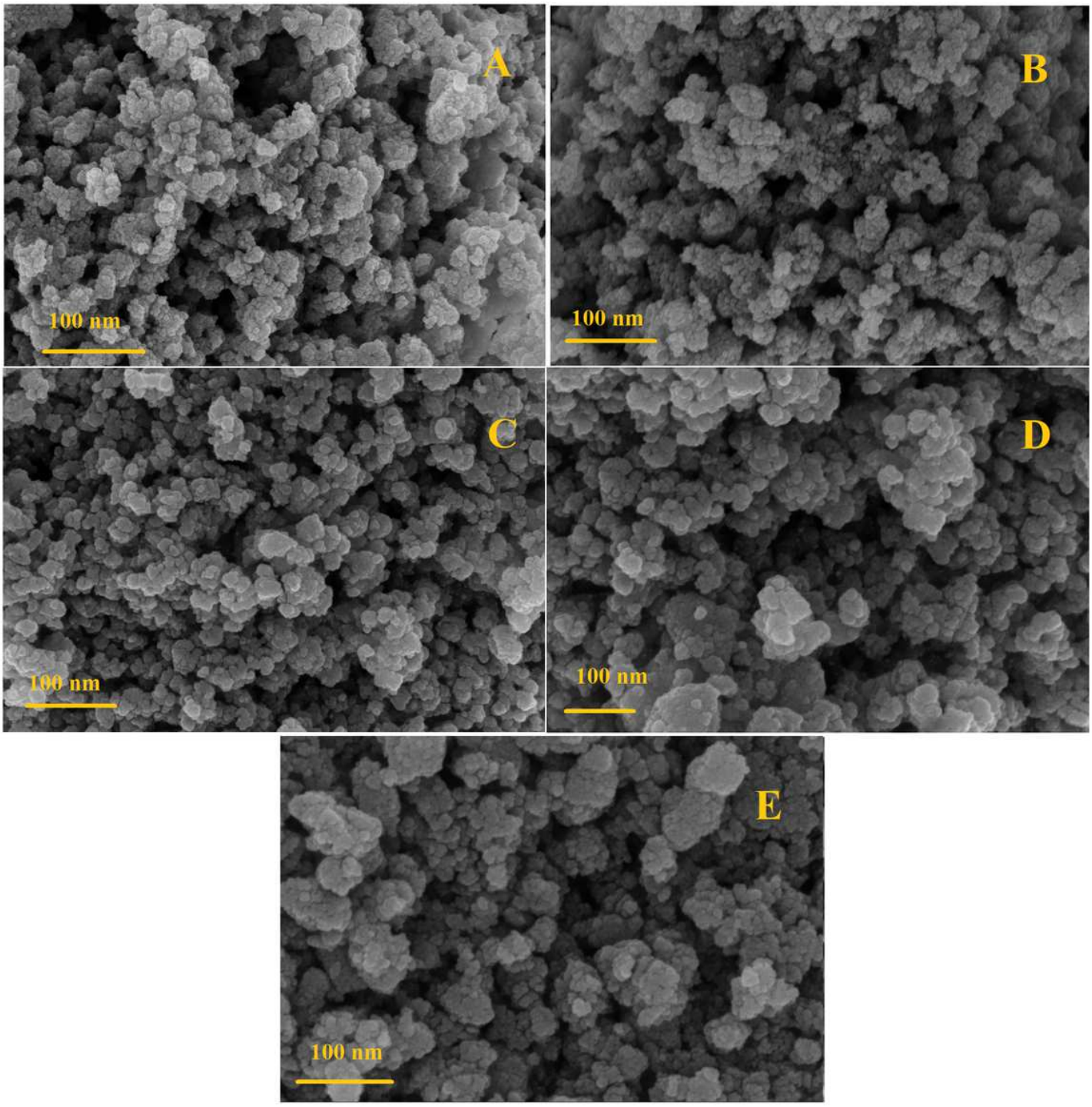

Figure 2

FESEM analysis spectra of A) undoped and Mg-TiO2 NPs B)0.2g C)0.4g D) 0.6g E)0.8g of Mg

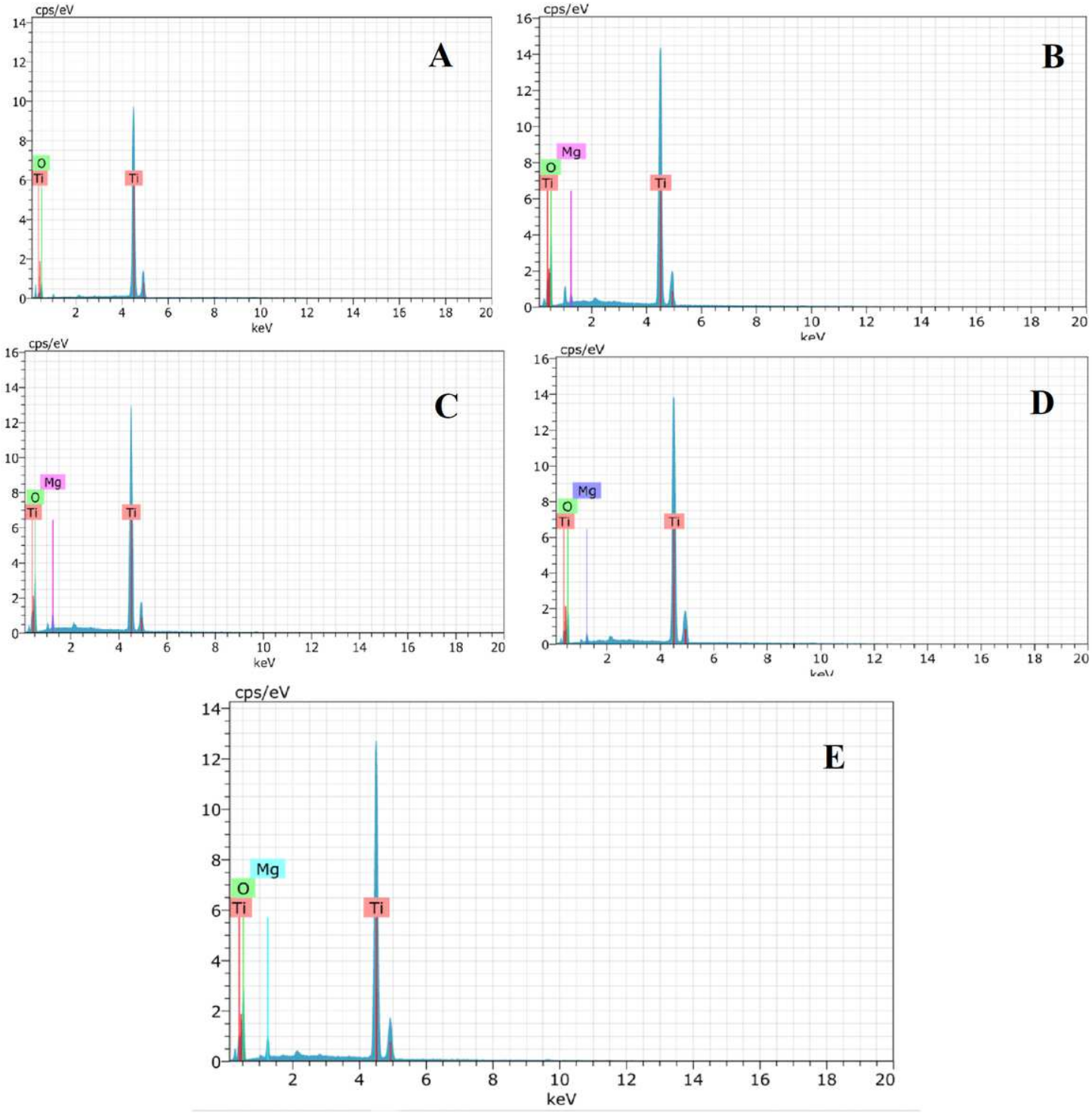

Figure 3

EDAX analysis of A) undoped and Mg-TiO2 NPs B)0.2g C)0.4g D) 0.6g E)0.8g of Mg

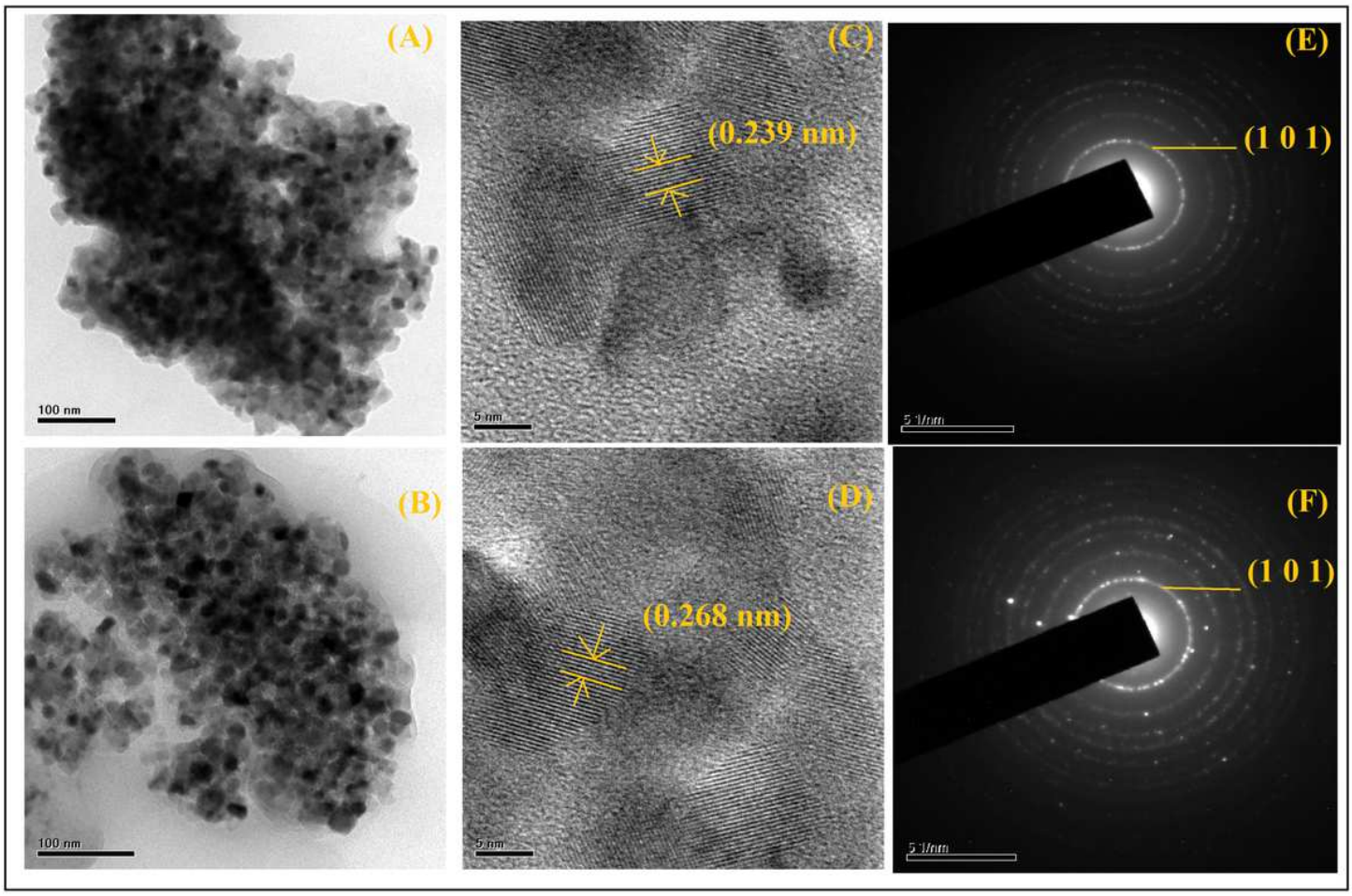

Figure 4

TEM analysis of A) undoped and Mg-TiO2 NPs B)0.2g C)0.4g D) 0.6g E)0.8g of Mg

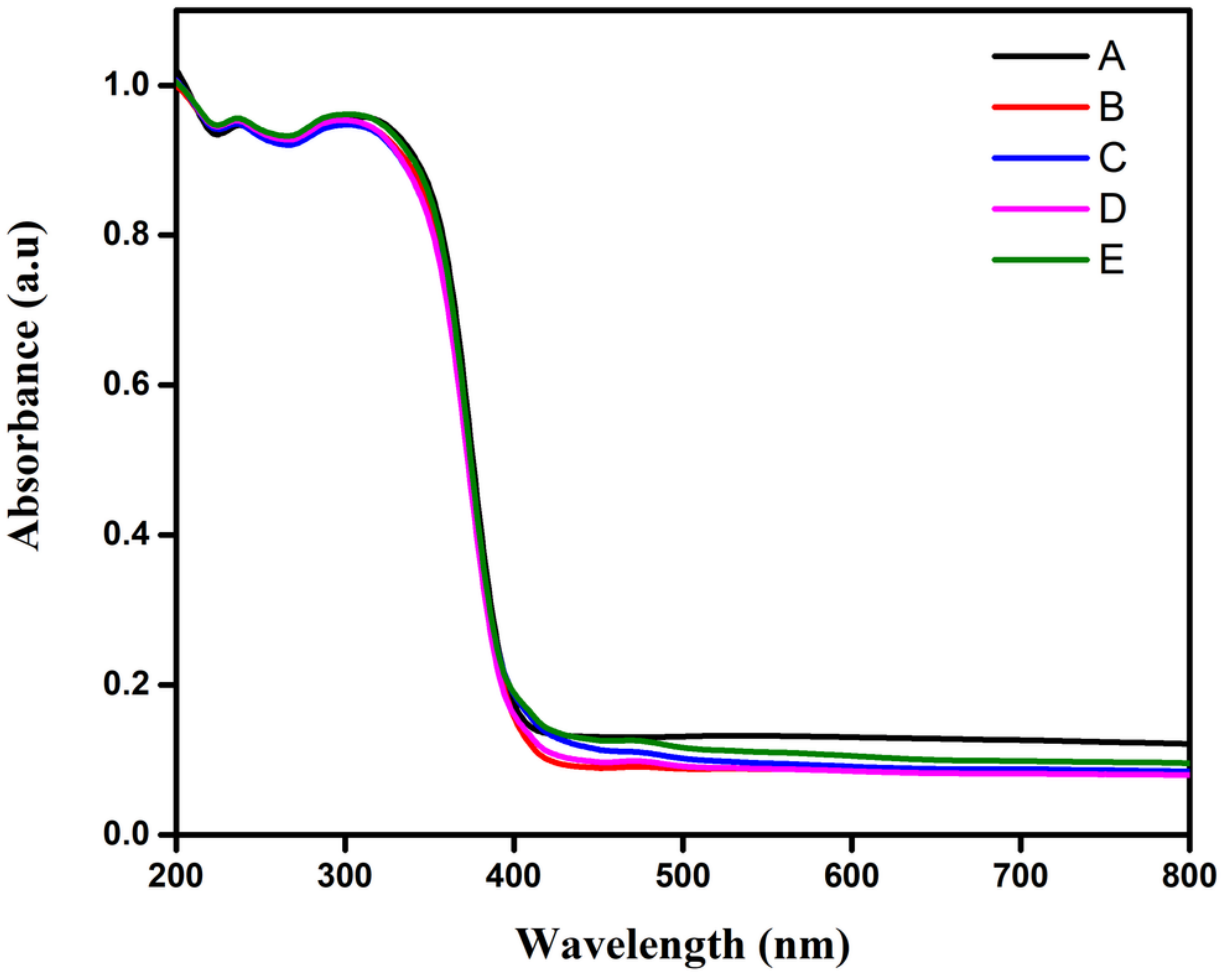

Figure 5

UV analysis of A) undoped and Mg-TiO2 NPs B)0.2g C)0.4g D) 0.6g E)0.8g of Mg

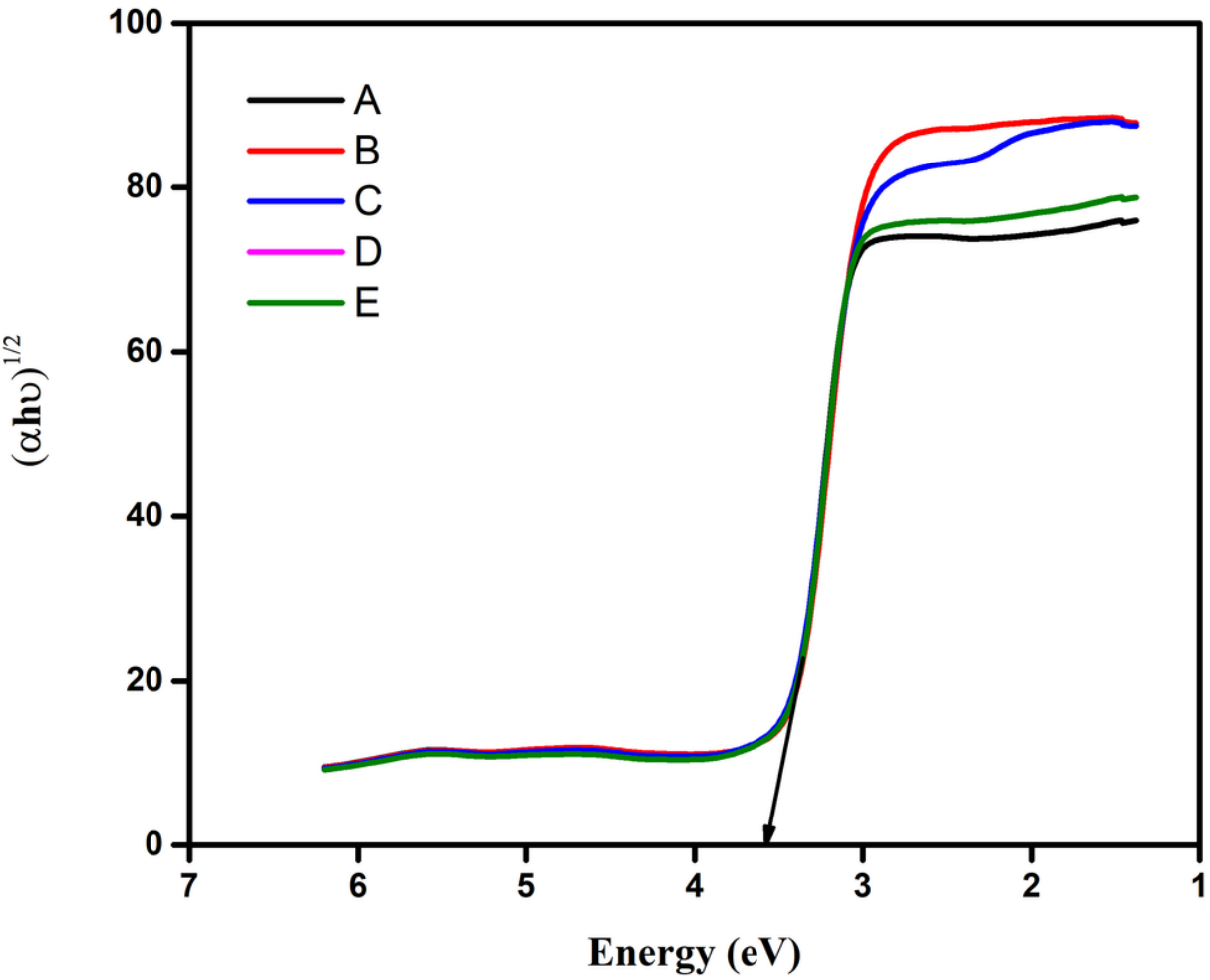

Figure 6

Tauc's Plot of A) undoped and Mg-TiO2 NPs B)0.2g C)0.4g D) 0.6g E)0.8g of Mg

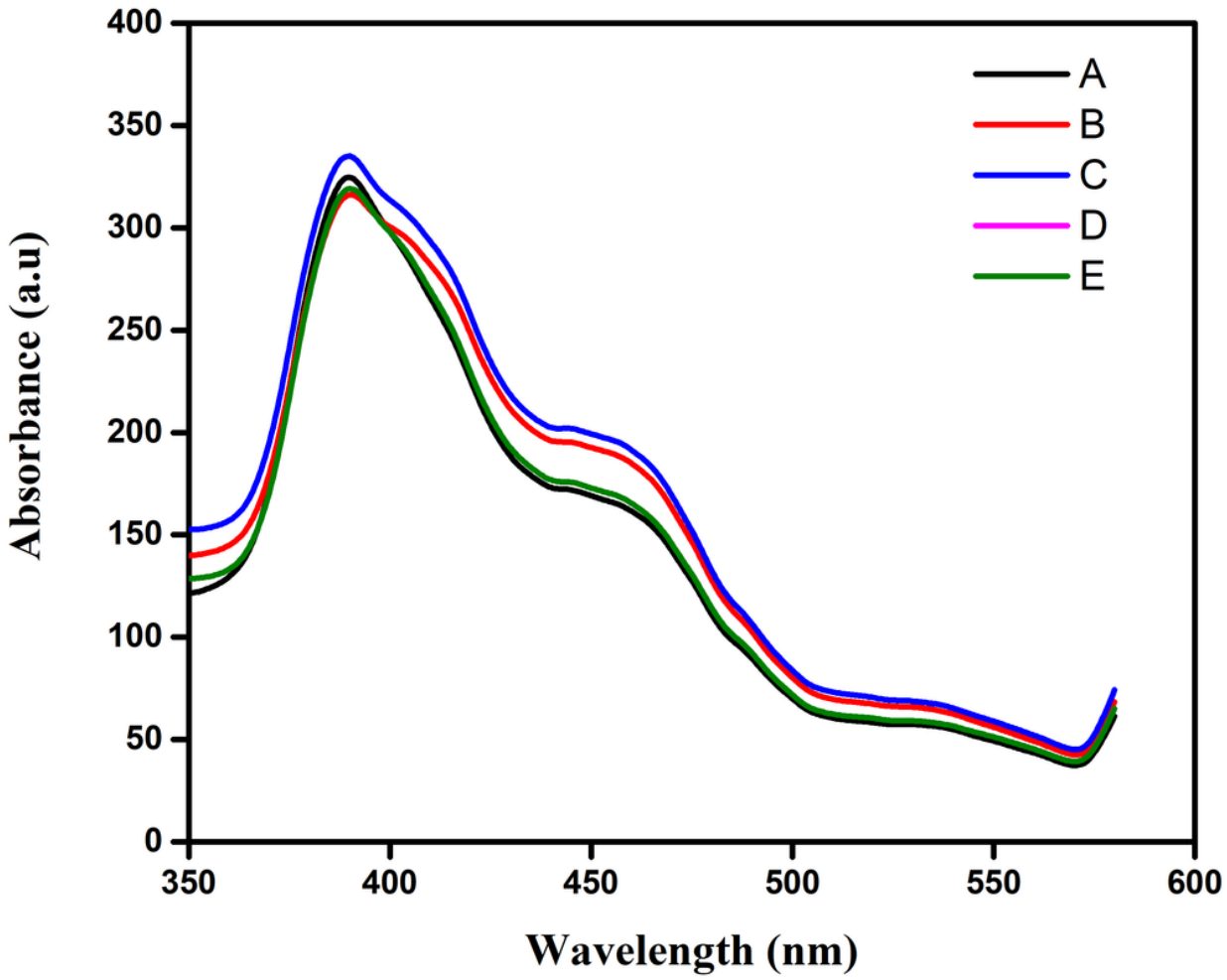

Figure 7

PL analysis of A) undoped and Mg-TiO2 NPs B)0.2g C)0.4g D) 0.6g E)0.8g of Mg

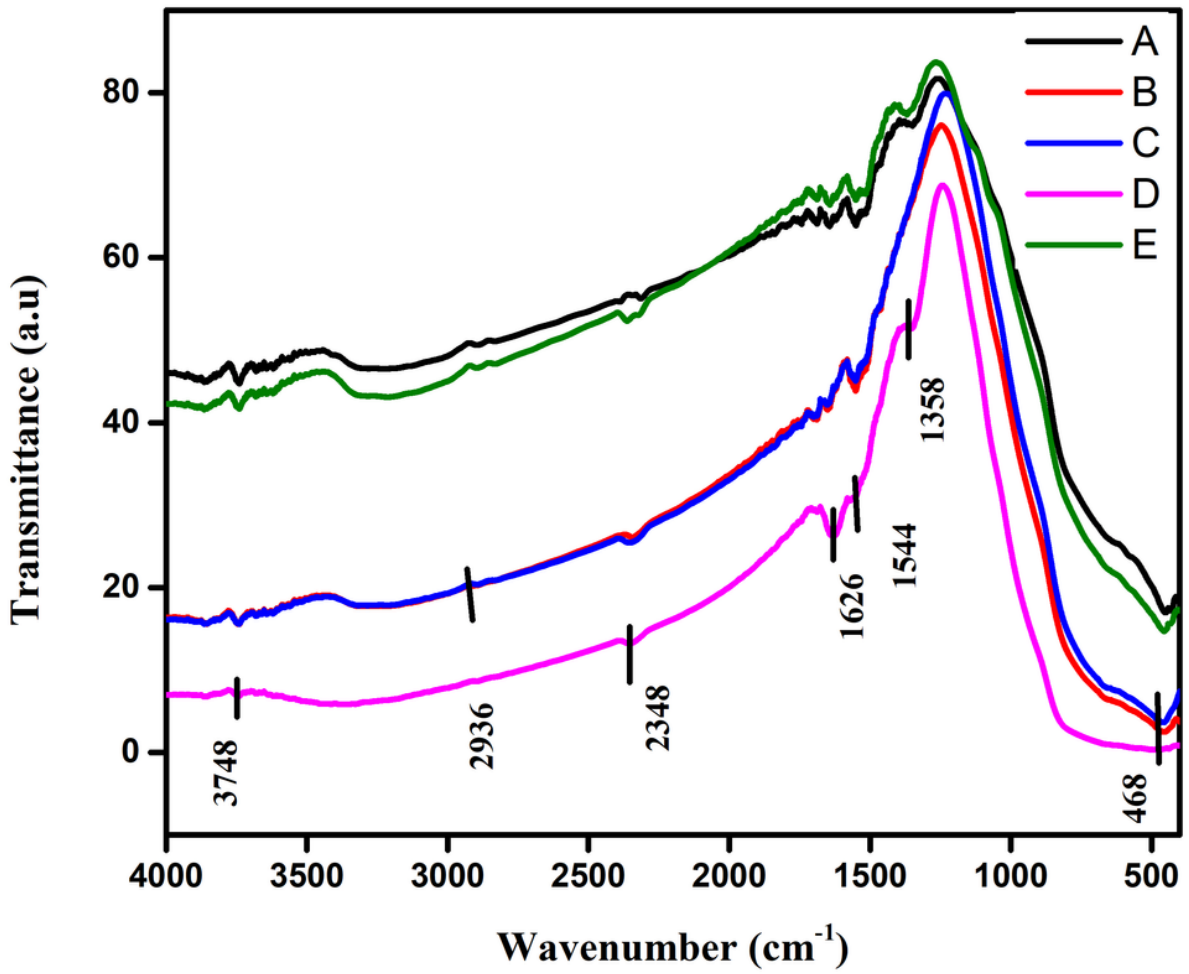

Figure 8

FTIR analysis of A) undoped and Mg-TiO2 NPs B)0.2g C)0.4g D) 0.6g E)0.8g of Mg

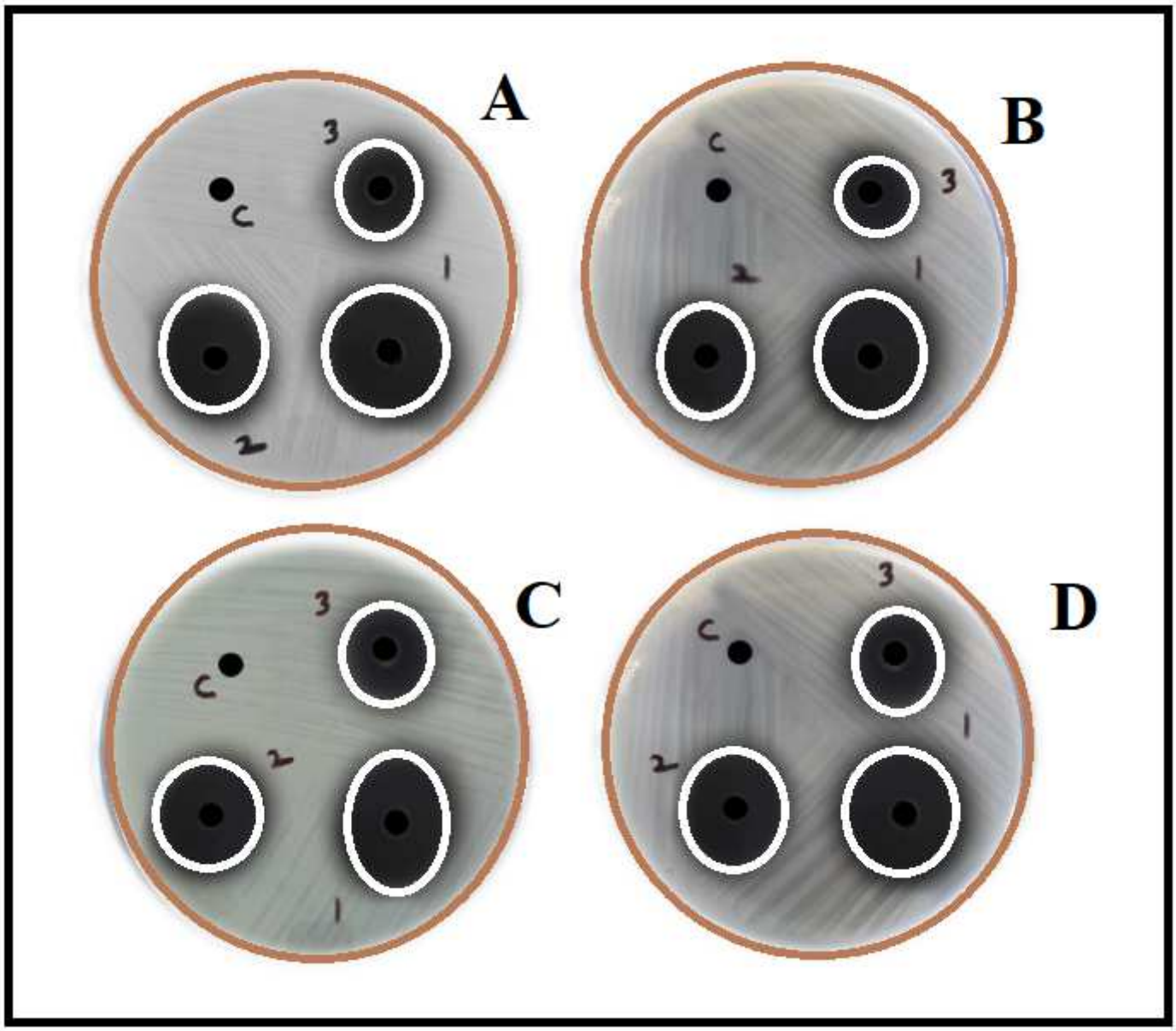

Figure 9

Zone of Inhibition of 1) undoped and 2) Mg-TiO2 NPs (0.2g) 3) Mg-TiO2 NPs (0.8g) A) Bacillus subtilis B) Staphylococcus aureus C) Pseudomonas aureginosa and D) Klebsiella pneumonia

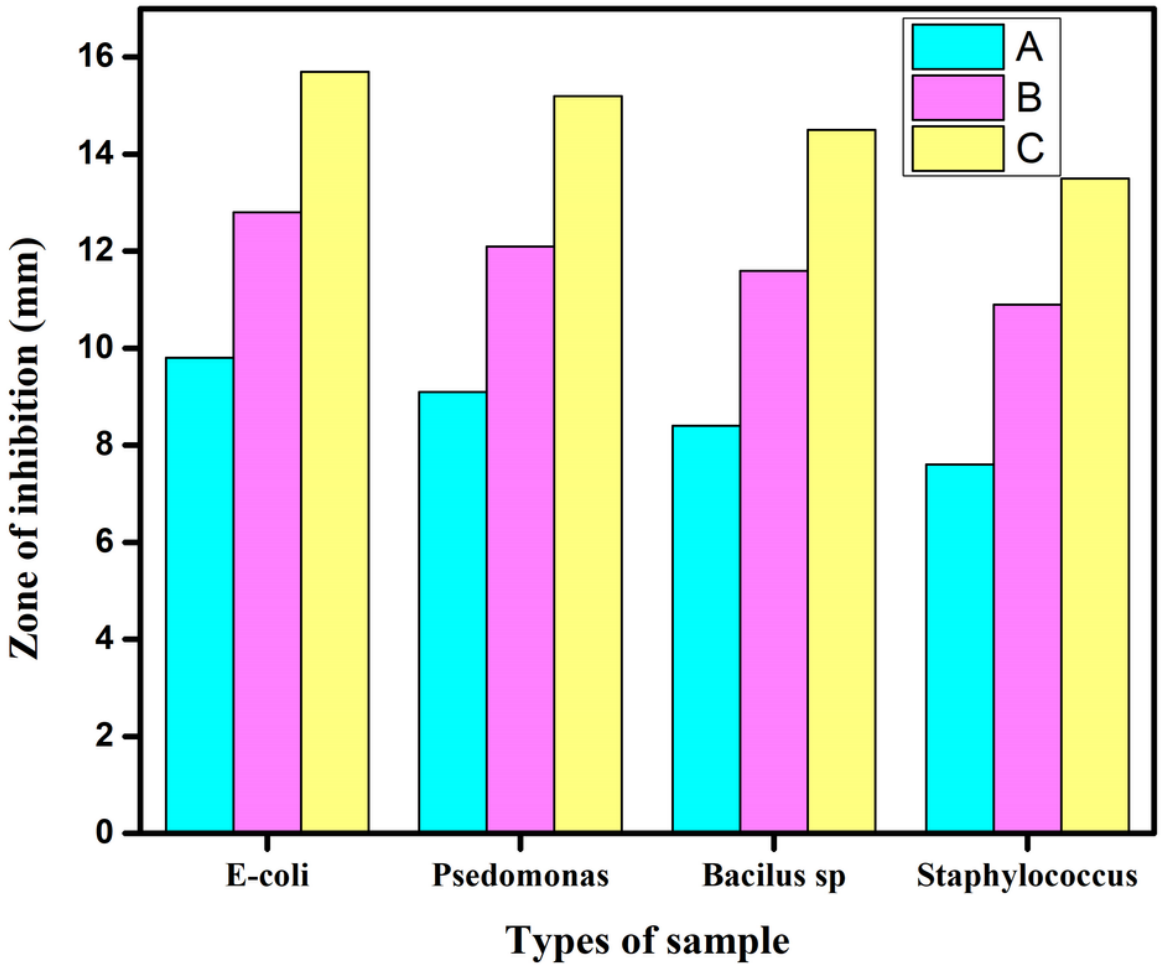

Figure 10

Antibacterial activity of A) undoped and B) Mg-TiO2 NPs (0.2g) C) Mg-TiO2 NPs (0.8g)

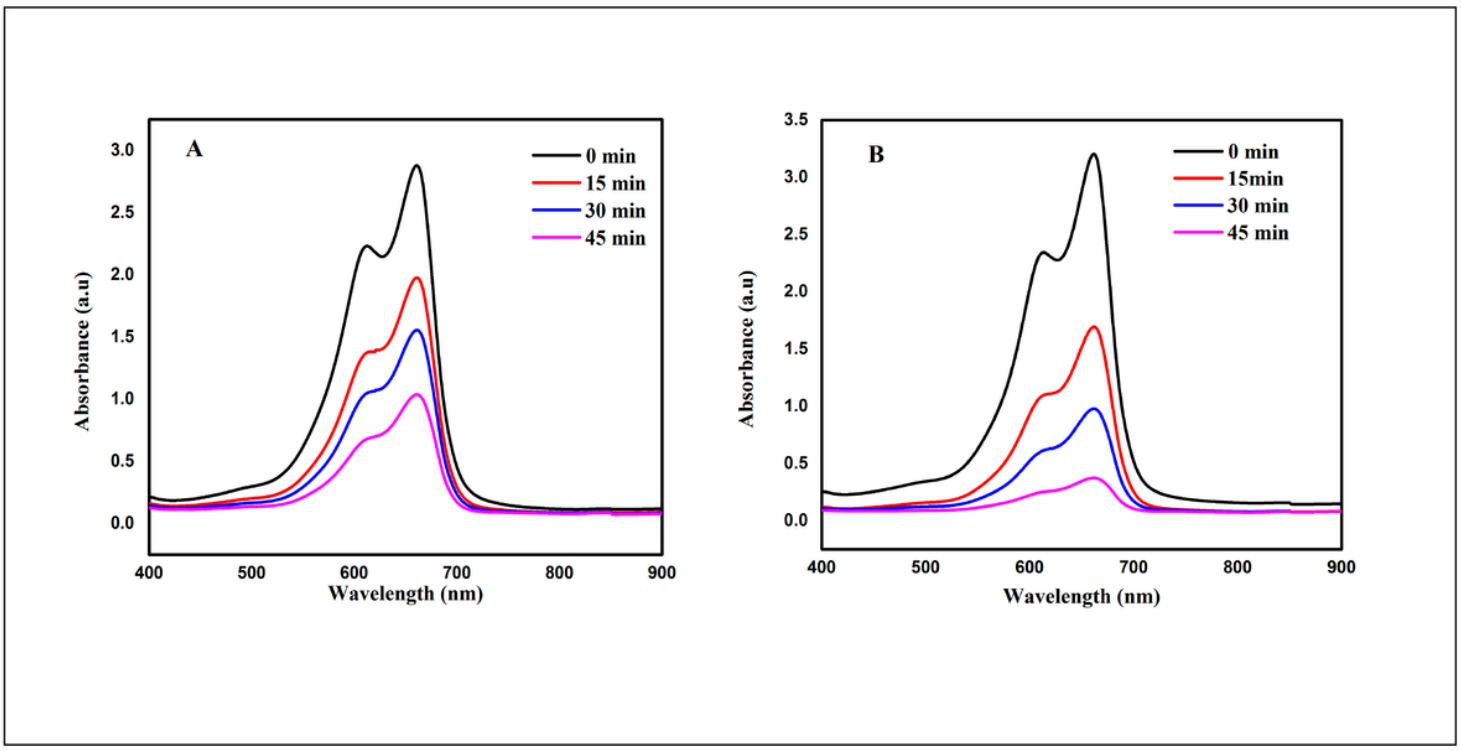

Figure 11

Photocatalytic degradation of A) undoped and B) Mg-TiO2 NPs (0.8g)

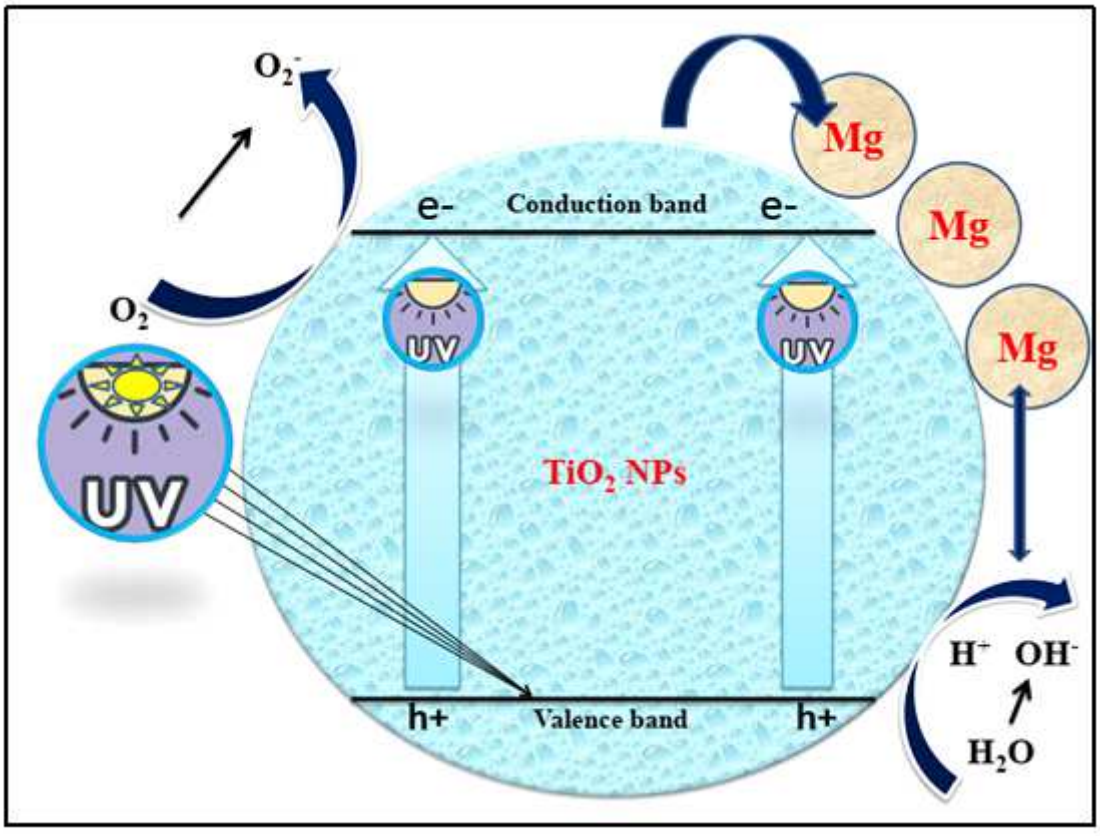

Figure 12

Photocatalytic mechanism of undoped and Mg-TiO2 NPs

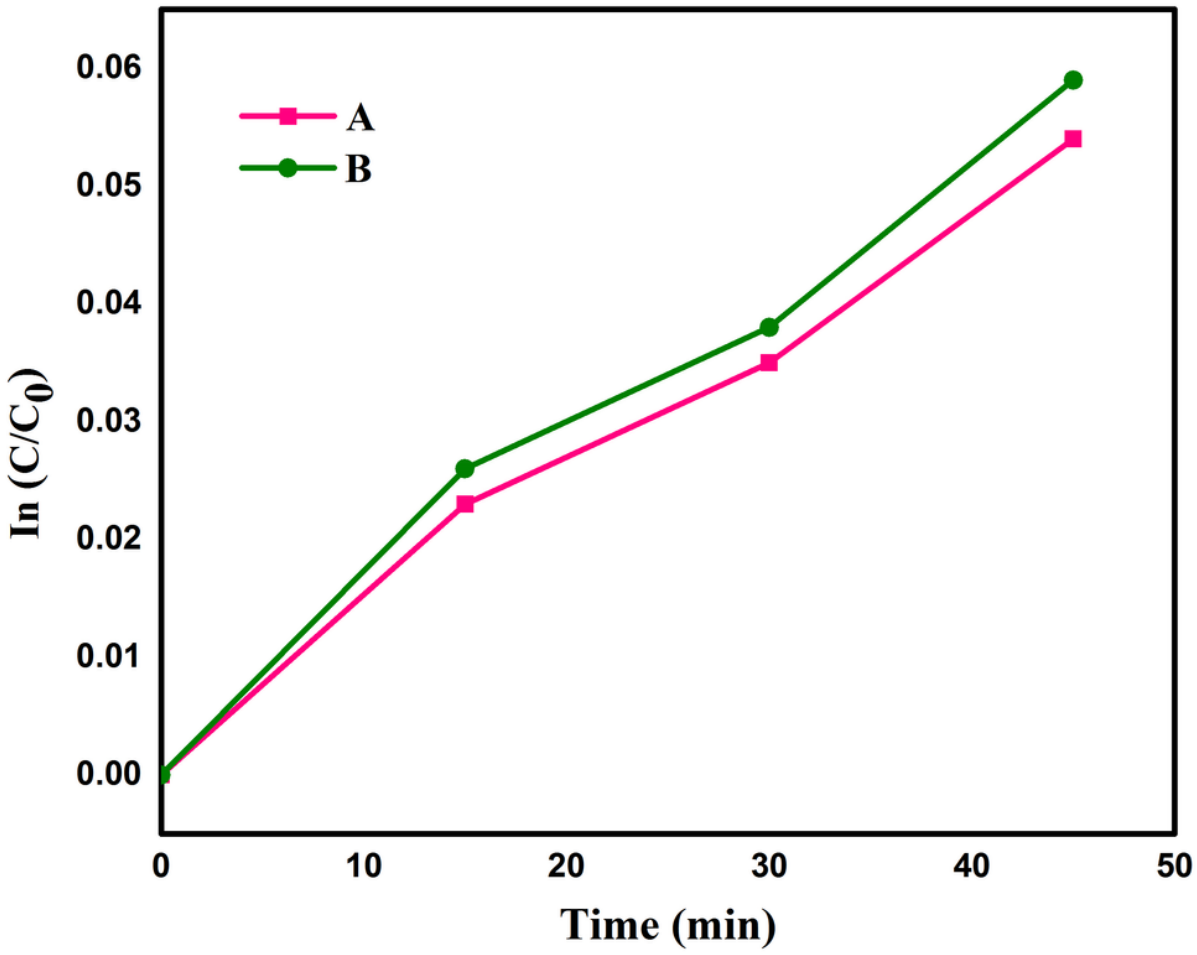

Figure 13

Rate constant for A) undoped and B) Mg-TiO2 NPs (0.8g)

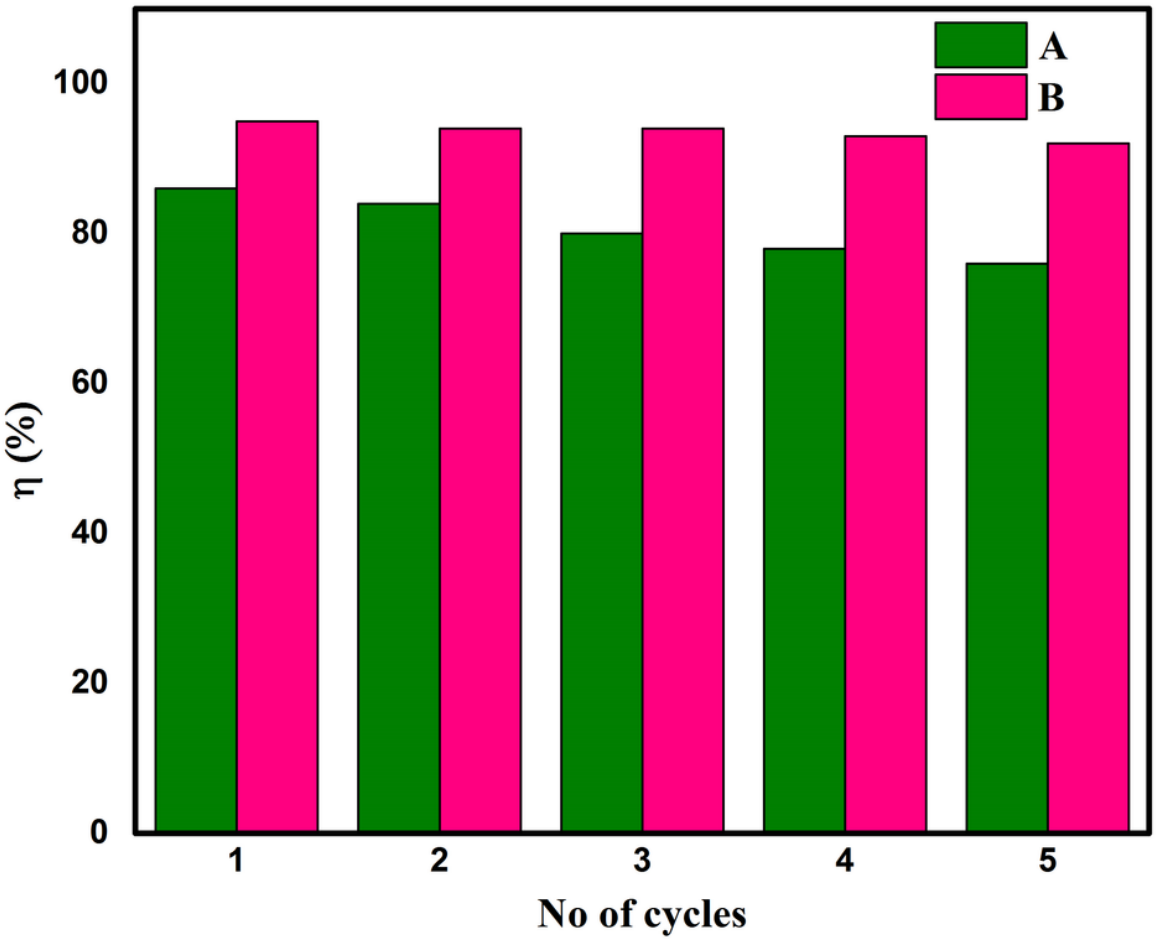

Figure 14

Degradation efficiency of A) undoped and B) Mg-TiO2 NPs (0.8g)